Review Article

ADVANCED PHOTONICS

# Engineering photonic angular momentum with structured light: a review

Jian Chen,[a] Chenhao Wan,[a,b] and Qiwen Zhan[a,*]
[a]University of Shanghai for Science and Technology, School of Optical-Electrical and Computer Engineering, Shanghai, China
[b]Huazhong University of Science and Technology, School of Optical and Electronic Information, Wuhan, China

**Abstract.** Structured light with inhomogeneous phase, amplitude, and polarization spatial distributions that represent an infinite-dimensional space of eigenstates for light as the ideal carrier can provide a structured combination of photonic spin and orbital angular momentum (OAM). Photonic spin angular momentum (SAM) interactions with matter have long been studied, whereas the photonic OAM has only recently been discovered, receiving attention in the past three decades. Although controlling polarization (i.e., SAM) alone can provide useful information about the media with which the light interacts, light fields carrying both OAM and SAM may provide additional information, permitting new sensing mechanisms and light–matter interactions. We summarize recent developments in controlling photonic angular momentum (AM) using complex structured optical fields. Arbitrarily oriented photonic SAM and OAM states may be generated through careful engineering of the spatial and temporal structures of optical fields. Moreover, we discuss potential applications of specifically engineered photonic AM states in optical tweezers, directional coupling, and optical information transmission and processing.

Keywords: photonic angular momentum; spin angular momentum; orbital angular momentum; transverse spin; transverse orbital angular momentum; spatiotemporal optical vortex.

Received Apr. 18, 2021; revised manuscript received Oct. 13, 2021; accepted for publication Oct. 15, 2021; published online Nov. 17, 2021.



[DOI: 10.1117/1.AP.3.6.064001]

## 1 Introduction

Light is a viable information carrier employing the various forms of light–matter interactions for numerous applications in data transmission, optical communications, photonics, and optoelectronics. In particular, optical measurement techniques, including interferometry, spectroscopy, and ellipsometry, determine and characterize the optical properties of materials or structures and are widely used in several fields of physics, materials science, microelectronics, biology, etc. Traditionally, light fields with simple spatial distribution such as plane waves and fundamental Gaussian beams have been employed in these applications. In recent years, structured light[1] has become an emerging approach in modulating and tailoring the three-dimensional (3D) distributions of a light beam in its multiple degrees of freedom (i.e., amplitude, phase, polarization ratio, and ellipticity) with high spatial diversity. The spatial diversity present within the cross section of structured light offers much higher degrees of freedom in optical system design, which in turn enable high-capacity information transmission or the specific shaping of intensity and phase distributions to achieve the desired optimized light–matter interactions, such as super-resolution imaging, optical tweezing, and optical nanofabrication. In this review, we focus on how structured light can be utilized to generate, tailor, structure, and modify the properties of light angular momentum (AM), sometimes in rather unexpected ways.

Similar to electrons, photons can carry two types of AM, namely orbital angular momentum (OAM) and spin angular momentum (SAM).[2–5] SAM is related to the circular polarization of the optical field [Fig. 1(a)],[6–8] whereas intrinsic OAM is associated with a helical wavefront [Fig. 1(b)].[9–14] In addition, extrinsic OAM also exists for optical fields propagating at a distance with respect to the coordinate origin [Fig. 1(b)]. Extrinsic OAM can be expressed as the cross product of the position vector $\mathbf{r}$ of the beam center and its linear momentum vector $\mathbf{P}$, where $\mathbf{P}$ is parallel to the mean wavevector $\langle \mathbf{k} \rangle$.[8,15] We will

*Address all correspondence to Qiwen Zhan, qwzhan@usst.edu.cn

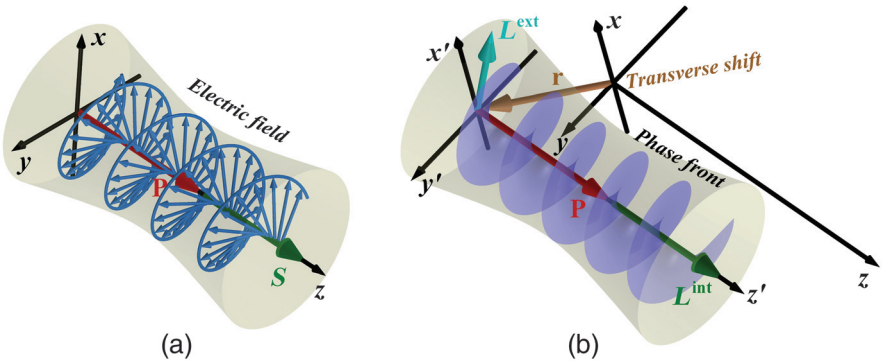


**Fig. 1** Angular momentum in paraxial optical fields: (a) longitudinal SAM of the right-handed circularly polarized field and (b) intrinsic longitudinal OAM with the helical wavefront illustrated with the purple surface. An extrinsic OAM arises from a shift with respect to the coordinate systems.

restrict our discussions of OAM to the intrinsic type, since the extrinsic OAM depends on the chosen coordinate system. As will be discussed in the following sections, both SAM and OAM are in parallel with the propagation direction of the optical beam under paraxial conditions. For differentiation purposes, we will refer to these two as longitudinal SAM and OAM.[16–26]

Under situations that involve strong focusing or evanescent waves, the situation can change dramatically, and AM with a component that is orthogonal to the propagation direction can be generated, which will be referred to as transverse AM. The transverse AM of light has gained increasing attention because of its unique physical characteristics.[27–41] The spin axis of the optical beam with purely transverse SAM is orthogonal to its propagation direction because of the existence of a longitudinal electric field component that is in the quadrature ($\pi/2$ phase difference) with respect to its transverse field components.[42–44] So far, the transverse SAM has been found to appear locally in three-dimensionally structured optical fields, including evanescent waves,[45] strongly focused field,[46,47] two-wave interference,[48] near-field radiation,[49] surface plasmon polaritons,[32,50–52] and wave-guide modes.[53–58] Moreover, arbitrarily oriented SAM states can be obtained by carefully engineering vectorial structured optical fields.[59]

Optical fields can be structured not only in the spatial domain but also in the spatiotemporal domain. This leads to the fairly recent discovery of transverse OAM. Through introducing a helical phase in the spatiotemporal domain, the spatiotemporal optical vortex (STOV) can be generated, which carries OAM perpendicular to the beam propagation direction.[60–62] Using a method similar to the conversion from the Hermite–Gaussian mode to the Laguerre–Gaussian mode with a cylindrical lens in the spatial domain, subwavelength focused STOV can be created through preconditioning both phase and amplitude distributions of the incident wave packet, paving the way for the study of transverse OAM with nanostructures and materials.[63]

Photonic AM enables distinctively different interaction mechanisms that may render important information about the materials or enable unique functionality that could not be realized in other ways. Hence, there is a need to develop methodologies and techniques to control, engineer, and optimize the photonic AM density distribution for specific applications. With the rapid advances in nanofabrication and optical field engineering, arbitrarily oriented photonic SAM and OAM states can be generated by customizing spatially and spatiotemporally structured light. In the following sections, we will discuss several of the latest theoretical and experimental investigations in this nascent research field to illustrate the concepts of generation, shaping, and optimization of photonic AM distributions using structured light, which will be followed by a brief overview of their applications in a few typical areas. We will begin with a brief mathematical description of the photonic AM employing the canonical momentum and spin densities. Then, we will illustrate how the SAM of the tightly focused field can be tailored by employing structured light as the incident pupil field of a high numerical aperture (NA) lens. A time-reversal methodology that can potentially be developed into a more universal approach is described to create diffraction limited optical focus with arbitrarily oriented photonic SAM states. Further, we will examine how a 3D polarization topology, namely the optical polarization Möbius strip, can be formed by the circularly polarized points in the tightly focused optical field with the presence of transverse SAM, and the approach to designing and optimizing similar topology with more complex trajectories and dynamic behaviors. Subsequently, we will turn our attention to the latest developments in the controllable generation of transverse OAM and how the OAM can be modified. Finally, typical applications of specifically engineered photonic AM states will be discussed, and future perspectives for this very nascent field will be presented.

## 2 Photonic Angular Momentum

To begin, we consider a monochromatic light wave with angular frequency $\omega$ and amplitude vectors $\mathbf{E}(\mathbf{r})$ and $\mathbf{H}(\mathbf{r})$ propagating in free space. For electromagnetic fields in dispersive media, exploiting the corresponding permittivity and permeability allows for modification of the following presented formulas.[64,65] The cycle-averaged energy density can be written as[66]

$$Q = \frac{g\omega}{2}(|\mathbf{E}|^2 + |\mathbf{H}|^2), \tag{1}$$

where the Gaussian unit $g = (8\pi\omega)^{-1}$. Correspondingly, the canonical momentum density of light is defined as[67,68]

$$\mathbf{P} = \frac{g}{2}\,\mathrm{Im}[\mathbf{E}^* \cdot (\nabla)\mathbf{E} + \mathbf{H}^* \cdot (\nabla)\mathbf{H}]. \tag{2}$$

Equation (2) shows that the canonical linear momentum density is related to the field vector of light to the second order. Meanwhile, the canonical OAM density can be written as

$$\mathbf{L} = \mathbf{r} \times \mathbf{P}. \tag{3}$$

For light waves with a helical phase, Eq. (2) presents a phase gradient term for Eq. (3), leading to the intrinsic OAM contribution. The helical phase in the transverse spatial domain causes the longitudinal average OAM,[69] while a helical phase variation in the spatiotemporal domain results in the transverse average OAM.[61–63] On the other hand, the SAM is connected to the vectorial nature of light[70] with a density given by

$$\mathbf{S} = \frac{g}{2}\,\mathrm{Im}(\mathbf{H}^* \times \mathbf{H} + \mathbf{E}^* \times \mathbf{E}). \tag{4}$$

From Eq. (4), it is apparent that the spin density is proportional to the local polarization ellipticity and parallel to the normal of the polarization ellipse.

The sum of the two AM densities given by Eqs. (3) and (4) gives the total AM density $\mathbf{J} = \mathbf{S} + \mathbf{L}$. Moreover, a paraxial polarized vortex beam can be written as[66]

$$\mathbf{E}(\rho, \phi, z) = A(\rho, z)\frac{\mathbf{e}_x + m\mathbf{e}_y}{\sqrt{1 + |n|^2}}\,\exp(jkz + j\ell\phi),$$
$$\mathbf{H} = \mathbf{e}_z \times \mathbf{E}, \tag{5}$$

where $m$ is a complex number used to characterize the polarization,[71] $\ell$ is the integer topological charge ($\ell = 0, \pm 1, \pm 2, \ldots$), $A(\rho, z)$ is the complex amplitude of the vortex beam, and $\mathbf{e}_x$, $\mathbf{e}_y$, and $\mathbf{e}_z$ are the unit vectors along the $x$, $y$, and $z$ axes in the Cartesian coordinate system, respectively. The average OAM $\overline{\mathbf{L}}$ and SAM $\overline{\mathbf{S}}$ for this beam can be shown as[66]

$$\frac{\overline{\mathbf{S}}}{Q} = \frac{\sigma\mathbf{k}}{\omega k}, \quad \frac{\overline{\mathbf{L}}}{Q} = \frac{\ell\mathbf{k}}{\omega k}, \tag{6}$$

where the helicity parameter $\sigma = 2\,\mathrm{Im}(m)/(1 + |m|^2)$, in which $\sigma = +1$ for right-handed circular polarization ($m = i$), $\sigma = -1$ for left-handed circular polarization ($m = -i$), and $\sigma = 0$ for linear polarization [$\mathrm{Im}(m) = 0$]. Hence, each photon in the right-handed (left-handed) circularly polarized beam possesses SAM of $+\hbar$ ($-\hbar$). In addition, each photon in the beam with a helical wavefront $\exp(i\ell\phi)$ carries OAM of $\ell\hbar$.

Based on Eq. (6), both SAM and OAM of paraxial beams are parallel with their propagation direction, known as the longitudinal AMs. However, under non-paraxial conditions or if evanescent fields are involved, there exists a field component along the propagation direction, although in most cases this longitudinal field component is not propagating. According to Eq. (4), the longitudinal field component leads to a transverse SAM component that is perpendicular to the propagation direction. In most cases, the transverse SAM component is negligible compared with the longitudinal counterpart. However, there is a possibility of dramatically increasing the transverse SAM component and making the SAM purely transverse via using focusing, interference, wave-guide modes, or specifically designed structured light, which can also be exploited to tailor the SAM local density with specific orientations, distributions, and topology. This shows the necessity of having a systematic approach to design the structured light to tailor the SAM for a specific application need, which will be illustrated in the following sections.

## 3 Tailoring the Spin Angular Momentum with Structured Light

The SAM of an optical field is associated with its polarization, as mentioned previously. Specifically, the SAM of paraxial beams has a simple structure that is along the propagation direction. However, it is feasible to tailor the local SAM with distributed textures for light fields with complex structures, which can be illustrated by the generation of purely transverse SAM (i.e., the so-called photonic wheel), as shown in Fig. 2.[46,72] A specially segmented quarter-wave plate (QWP) is employed to convert the linearly polarized incident beam into the circular polarization state with opposite chirality in the two halves of the beam, as shown in Fig. 2(a), which leads to a structured field in polarization. A high NA objective lens (NA = 0.9) is used to focus the structured field, in which the longitudinal SAM components $J^+$ and $J^-$ cancel each other, and their transverse counterparts are retained to form a purely transverse SAM in the focal region, as shown in Fig. 2(b). It should be noted that the transverse SAM is generated due to the creation of a longitudinal electrical field component under high NA focusing conditions. In addition, a nanoparticle is used as a probe to scan through the focal field to experimentally characterize the polarization state of the focused field, as shown in Fig. 2(c). The Mie scattering field at each scanned position is gathered by an immersion-type objective lens with NA of 1.3 and measured by a camera, which allows the derivation of the three complex electrical field components. The reconstructed distributions of $|\mathbf{E}_{\mathrm{tot}}|^2$, $|\mathbf{E}_x|^2$, $|\mathbf{E}_y|^2$, and $|\mathbf{E}_z|^2$ of the focused field are depicted in Figs. 2(d)–2(g), respectively. The insets in Figs. 2(e)–2(g) present the corresponding relative phases $\Phi_x$, $\Phi_y$, and $\Phi_z$. Obviously, the phase difference $\Delta\Phi_{y,z} = \Phi_y - \Phi_z$ is a value of $\{\pi/2, -\pi/2, -3\pi/2\}$, $\Delta\Phi_{x,z} = \Phi_x - \Phi_z$ is a value of $\{\pi/2, -\pi/2, 3\pi/2\}$, whereas $\Delta\Phi_{x,y} = \Phi_x - \Phi_y$ is a value of $\{\pi, 0, -\pi\}$. Therefore, the spin axis of the focused field is orthogonal to the $z$ direction, namely, the SAM of the focal field is purely transverse.

The aforementioned example demonstrates the generation of purely transverse SAM by focusing the structured light. However, the structured light used is rather simple, the purely transverse SAM occurs at a very low-intensity region within the focus, and the focal spot is not diffraction limited. Thus, it is natural to ask the question, how we can optimize and efficiently generate such SAM distribution? More generally, how can we generate SAM distribution efficiently with an arbitrarily desired orientation? A versatile time-reversal method is demonstrated to address these questions.[73–75] As shown in Fig. 3(a), two orthogonal electric dipoles are exploited to simulate a focal field with SAM along a preconditioned orientation. Since we are interested in SAM, we will give a $\pi/2$ phase difference between the two dipoles. Dipole 1 is placed in the $yz$ plane, and its oscillation direction has an angle of $\theta_1$ relative to the negative direction of the $z$ axis; meanwhile, the oscillation direction of dipole 2 is along the $x$ axis. The pupil field distribution can be found through coherently superposing the radiation fields from the two dipoles, which in turn will be the required incident field

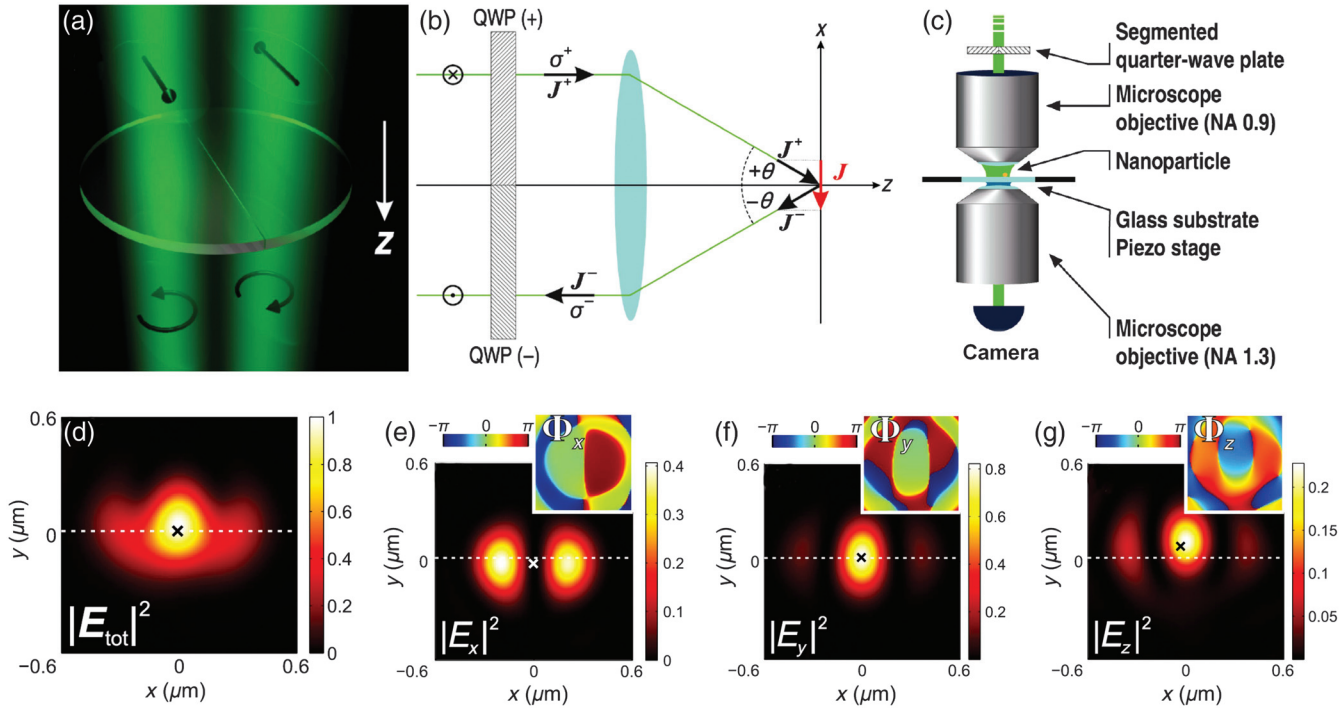


**Fig. 2** Generation of the transverse SAM in highly confined field. (a) A segmented QWP is adopted to obtain the desired incident beam. (b) Schematic of tightly focusing the incident field. (c) The experimental setup to generate and characterize the transverse SAM of the focused field. The reconstructed distributions of $|\mathbf{E}_{tot}|^2$, $|\mathbf{E}_x|^2$, $|\mathbf{E}_y|^2$, and $|\mathbf{E}_z|^2$ of the focal field are depicted in (d)–(g), respectively, and the insets present the corresponding relative phases. Panels (a)–(c) are reproduced with permission from Ref. 46; (d)–(g) are reproduced with permission from Ref. 72.

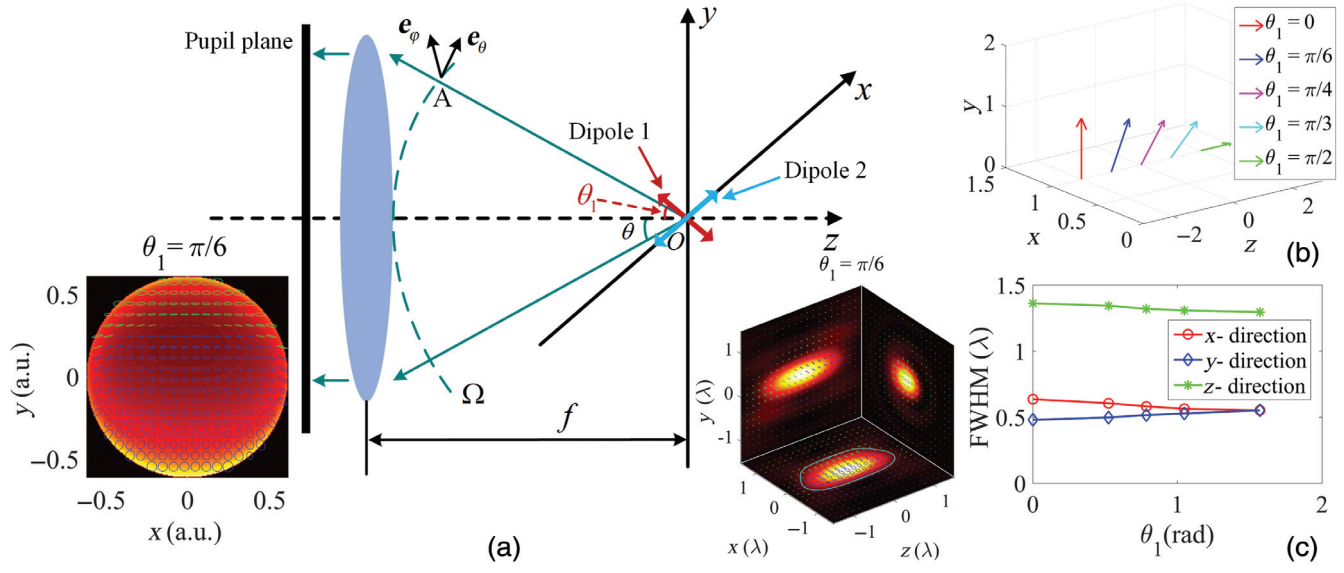


**Fig. 3** Spin orientation control based on the time-reversal method. (a) Schematic of the inverse calculation method. The insets present the projections of the focal field on three orthogonal cross sections and its corresponding incident structured pupil field for $\theta_1 = \pi/6$. (b) Evolution of the spin axis rotation in the $yz$ plane. (c) The beam sizes of focal fields. Figure reproduced with permission from Ref. 75.

for generating the highly confined focal field with the prescribed SAM. According to the dipole antenna theory,[76] and taking the apodization function of the lens into consideration (for a sine condition lens, the apodization function is $\sqrt{\cos\theta}$), and the required incident pupil field could be derived as

$$\begin{aligned}\mathbf{E}_i(r,\varphi) &\propto \frac{1}{\sqrt{\cos\theta}}\cdot(A\cdot\mathbf{e}_x + B\cdot\mathbf{e}_y),\\ A &= e^{j\pi/2}(\cos\theta_1\sin\theta\cos\varphi + \sin\theta_1\cos\varphi\sin\varphi\\ &\quad -\sin\theta_1\cos\theta\sin\varphi\cos\varphi) - \cos\theta\cos^2\varphi - \sin^2\varphi,\\ B &= e^{j\pi/2}(\cos\theta_1\sin\theta\sin\varphi - \sin\theta_1\cos^2\varphi\\ &\quad -\sin\theta_1\cos\theta\sin^2\varphi) - \cos\theta\cos\varphi\sin\varphi + \sin\varphi\cos\varphi.\end{aligned} \tag{7}$$

The vectorial Debye theory can be employed to confirm the SAM distributions within the focused electric field.[43,44] As an example, the structured illumination field at the pupil and the intensity and SAM of the focal field on three orthogonal cross sections for $\theta_1 = \pi/6$ are shown in the inset of Fig. 3(a). Meanwhile, the results in Figs. 3(b) and 3(c) clearly show that SAM distributions with arbitrary spatial orientation within diffraction limited focal dimensions in the transverse plane and beyond the diffraction limited dimension along the longitudinal direction can be realized by properly designing the structured pupil illumination field.[75]

## 4 Optical Polarization Möbius Strip

The structured light can be used to create more complicated spin topology and not just tailor the SAM with a prescribed orientation. The local field vector may rotate around any direction that gives rise to spatially inhomogeneous polarization states, owing to the emergence of the longitudinal electric field component. Within an optical field with inhomogeneous polarization distribution, polarization singularities may appear either as circular polarization or linear polarization.[77,78] In 3D space, polarization singularities can construct $C$ lines or $L$ lines. Tracing the 3D polarization ellipses along a small trajectory surrounding a single $C$ line can render a Möbius strip topology.[79]

The Möbius strip is a non-orientable surface that has only one side. Bauer et al. studied tightly focused light fields generated from a $q$-plate, which is an inhomogeneous and birefringent liquid crystal plate with electrically controlled phase retardation, and discovered Möbius strip topology that can be tuned by $q$-plate parameters.[79] The $q$-plate can be used to generate various structured light fields.[80] When the phase retardation is $\pi$, the $q$-plate changes the handedness of the spin of an incident beam, and the outgoing beam gains an OAM of $2q$, where $q$ is the topological charge of the $q$-plate pattern. When the phase retardation is not $\pi$, the $q$-plate transforms a circularly polarized Gaussian beam into a Poincaré beam. In the cross section of a Poincaré beam, the space variant polarization states cover the entire Poincaré sphere. Three major polarization topologies (lemon, star, and monstar) can be generated through a plate in the plane orthogonal to the direction of beam propagation. In Fig. 4(a), a Poincaré beam with a star-shaped $-1/2$ polarization topology generated from the $q$-plate is shown as the color inset and is tightly focused by a microscope objective. The same technique using a spherical gold nanoparticle for the photonic wheel characterization can be employed to characterize the complex electric field distributions in the focal area. The scattered light as well as the transmitted light is collected for 3D field reconstruction.

The space-varying polarization states are represented by the following equations:[77]

$$\begin{aligned}\boldsymbol{\alpha} &= \frac{1}{\left|\sqrt{\mathbf{E}\cdot\mathbf{E}}\right|}\,\mathrm{Re}\left(\mathbf{E}^*\sqrt{\mathbf{E}\cdot\mathbf{E}}\right),\\ \boldsymbol{\beta} &= \frac{1}{\left|\sqrt{\mathbf{E}\cdot\mathbf{E}}\right|}\,\mathrm{Im}\left(\mathbf{E}^*\sqrt{\mathbf{E}\cdot\mathbf{E}}\right),\\ \boldsymbol{\gamma} &= \mathrm{Im}(\mathbf{E}^*\times\mathbf{E}),\end{aligned} \tag{8}$$

where $\boldsymbol{\alpha}$ is the major axis of the 3D polarization ellipse, $\boldsymbol{\beta}$ is the minor axis of the 3D polarization ellipse, and $\boldsymbol{\gamma}$ is the normal to the polarization ellipse. In addition, $\boldsymbol{\alpha}$, $\boldsymbol{\beta}$, and $\boldsymbol{\gamma}$ are line fields rather than vector fields due to the sign ambiguity associated with the square roots. By purposefully assigning identical signs for the square roots, these line fields turn into vector fields, and $\boldsymbol{\alpha}$ is chosen to form the polarization topology. The $C$ line is formed by points where the major and minor axes degenerate. Following the major axis of the 3D polarization ellipse along a small closed path surrounding the $C$ line in the focal plane, it is discovered that the major axis undergoes a twist and forms a Möbius strip in 3D space.

A tightly focused Poincaré beam with a topological charge of $-1/2$ gives rise to a Möbius strip with three half twists, as shown in Fig. 4(b). Then, changing the topological charge to $-3/2$ results in five half twists in the focal plane, as shown in Fig. 4(c). The Möbius strip polarization topology exists not only in transmitted optical fields but also in scattered fields. The scattered fields from a silicon nanoparticle form a Möbius strip in any curve surrounding a $C$ line, as shown in Fig. 4(d).[81]

The kind of structured light created with a $q$-plate is certainly limited and may not be optimized for a specific desired topology or application. Much more complicated Möbius strip polarization topologies have been demonstrated through tailoring all three electric field components along prescribed trajectories in the focal region.[82] A Fourier transform relationship based on the Debye integral is established between the incident plane and the focal plane to tailor the polarization topology.[83] Moreover, exotic Möbius strip polarization topologies such as a figure "8" shaped twin Möbius strip and a circular Möbius strip with changing twisting speed are obtained by iterating back and forth between the two planes, as shown in Figs. 5(b) and 5(c).

In addition, aside from the trajectory of the Möbius strip, its twisting rate can also be manipulated. Figure 5(e) presents the intensity distributions in the focal area with varying twisting rates, in which the circular trajectory is divided into two halves denoted in solid white and dashed white curve lines, respectively. They are also represented as red and black curved lines in Fig. 5(f), respectively. The major axes of the polarization ellipses following the circular trajectory are plotted in blue and green to denote the orientation. The Möbius strip polarization topology along the black semicircle twists at a rate approximately twice that of the red semicircle.

From above discussions, we can infer that the optical Möbius strip certainly demonstrates the capability of customizing and characterizing the 3D polarization topology on a subwavelength scale, which may be useful for the polarization-sensitive

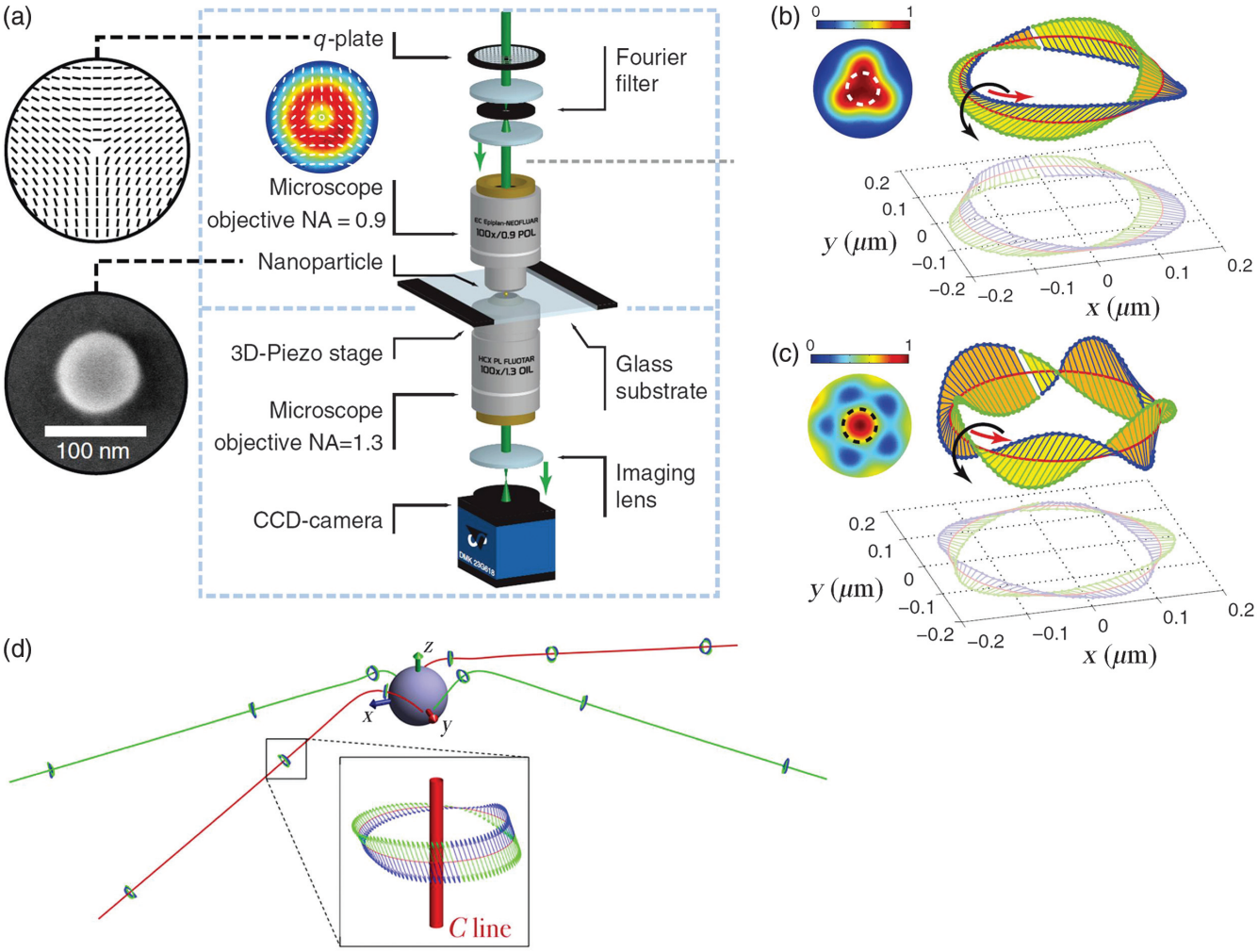


**Fig. 4** Generation of the optical Möbius strip polarization topology. (a) Schematic of the experimental setup to tightly focus the optical fields generated from a *q*-plate. (b) Experimentally generated Möbius strip polarization topology with three half twists in the focal plane. (c) Experimentally measured Möbius strip polarization topology with five half twists in the focal plane. (d) Scattered fields from a silicon nanoparticle form a Möbius strip in any curve surrounding a *C* line. Panels (a)–(c) are reproduced with permission from Ref. 79. Panel (d) is reproduced with permission from Ref. 81.

nanofabrication and light–matter interaction. We choose the Möbius strip as an example in illustrating the possibility of tailoring SAM distributions in an extremely sophisticated manner based on the recent advances made in the generation of structured light with spatial light modulators (SLMs) or metasurface devices.

## 5 Shaping Photonic Orbital Angular Momentum with Spatiotemporally Structured Light

So far, we have limited the discussion on engineering the SAM density distributions using spatially structured light. From Eq. (6), it is apparent that the OAM of an optical beam is longitudinal (i.e., along the propagation direction) under the paraxial condition. The possibility of having a pure transverse OAM that is perpendicular to the propagation direction is of major interest. Recently, the research on photonic OAM demonstrated the link between polychromatic spiral phase in the spatiotemporal domain and transverse OAM,[60–62] indicating that structuring the light in the spatiotemporal domain as opposed to strictly in the spatial domain is needed. Although it is straightforward to apply a twisted phase to the cross section of a beam to obtain a longitudinal OAM, it is non-intuitive to acquire a twisted phase in the spatiotemporal plane in a similar way in order to achieve a transverse OAM. Fortunately, a spiral phase can be conserved through two-dimensional Fourier transform. Therefore, transverse OAM can be generated after two-dimensional Fourier transform from the spatiotemporal-frequency plane to the spatiotemporal plane.[84]

Figure 6(a) shows the experimental setup for generating and characterizing a chirped wave packet embedded with a spatiotemporal vortex and transverse OAM using an in-house-built spatiotemporal wave packet generator that is composed of a diffraction grating, a cylindrical lens, and an SLM.[85] The light passes through the grating and cylindrical lens and illuminates

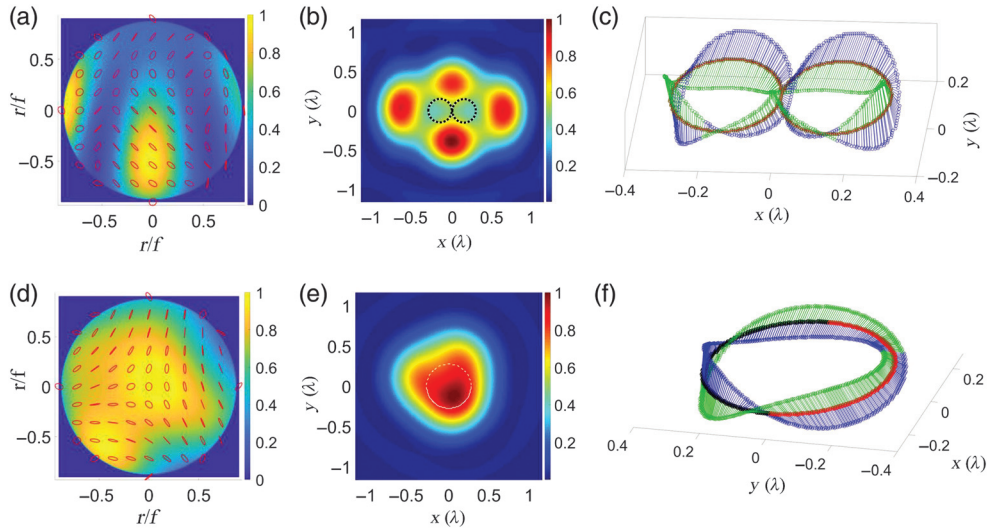


**Fig. 5** Generation of exotic optical Möbius strip polarization topology. (a) The intensity and polarization distributions in the pupil plane for the generation of an "8"-shaped twin Möbius strip. (b) Generation of an "8"-shaped twin Möbius strip in the focal area. The total intensity distributions in the focal plane with a prescribed "8"-shaped path denoted in the dashed black line. (c) The polarization topology along the red "8"-shaped path. (d) The intensity and polarization distributions in the pupil plane for the generation of a circular Möbius strip with changing twisting speed. (e) Generation of a circular Möbius strip with changing twisting speed in the focal region. (f) The two halves are plotted in red and black, respectively. The twisting rate of the black is twice that of the red half. Figure reproduced with permission from Ref. 82.

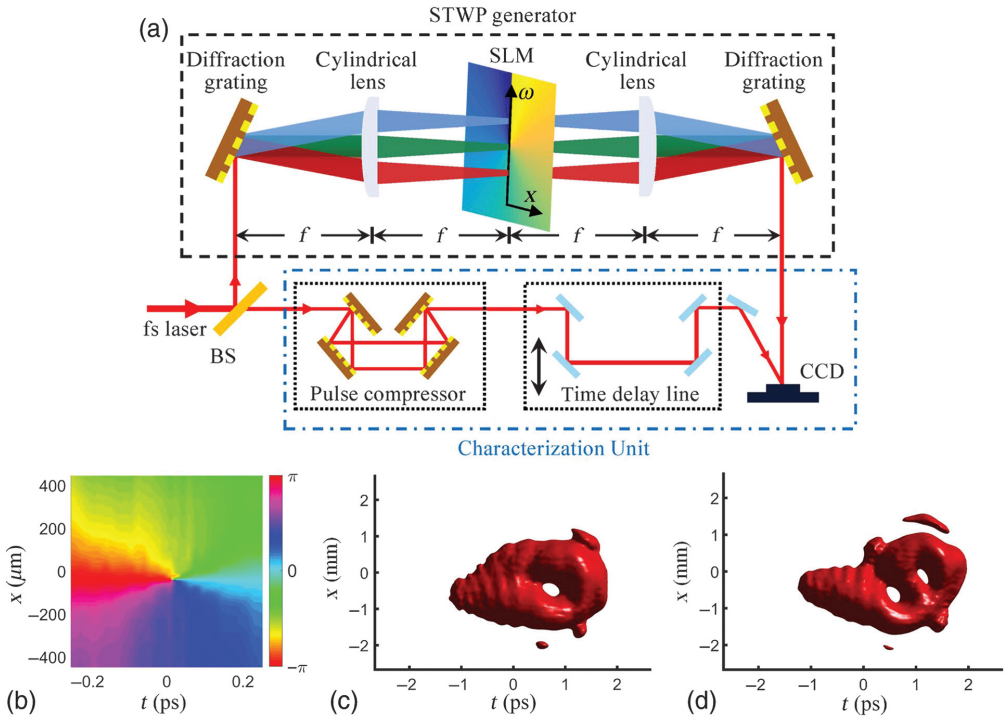


**Fig. 6** STOV with transverse OAM. (a) Experimental generation based on an SLM and characterization based on interference with a femtosecond reference pulse. (b) Reconstructed spatiotemporal phase distribution. (c) Measured 3D iso-intensity profile of a spatiotemporal vortex of $\ell = 1$. (d) Measured 3D iso-intensity profile of a spatiotemporal vortex of $\ell = 2$. Figure reproduced with permission from Ref. 61.

the SLM plane, which is considered as the spatiotemporal frequency plane. The SLM applies a controllable spiral phase that can be maintained after a spatiotemporal Fourier transform. The wave packet is analyzed by interfering with a probe pulse that is split from the fiber laser and dechirped through a grating pair using the characterization unit shown in Fig. 6(a).

The 3D optical field structure of the chirped wave packet in Fig. 6(a) is reconstructed based on the interference fringe patterns. Meanwhile, the reconstructed spatiotemporal phase distribution that is a spiral phase with topological charge 1 is shown in Fig. 6(b), and the 3D isointensity surfaces of the spatiotemporal vortices of topological charges 1 and 2 are shown in Figs. 6(c) and 6(d), respectively.[61,86] The experimental results clearly demonstrated the generation of STOV with purely transverse OAM by spatiotemporally structuring the light with a spiral phase.

The transverse OAM carried by a spiral spatiotemporal phase provides an extra degree of freedom for the applications that rely on exploiting optical OAM. In addition, this development can arbitrarily control the spatial orientation and density distribution of OAM. Several reports discussing the generation of arbitrarily oriented OAM through spatiotemporal coupling were published while this paper was in preparation.[87–89] Finally, further research into the spatially and spatiotemporally structured light[87,90] will offer novel opportunities to study the spin Hall effect, quantum entanglement, second harmonic generation, Kerr effect, and spin–orbital AM coupling based on spatiotemporal optical fields.

## 6 Fast Modulation of Orbital Angular Momentum in Temporal Domain

To this point, we have focused the discussions on engineering spatial characteristics of SAM and OAM, specifically the spatial orientation of AM. On the other hand, tailoring the temporal characteristics of AM, which involves the generation of ultrafast optical pulses with rapidly varying OAM characteristics in time, has gained increasing attention in recent years. To date, most research dealt with the static OAM of optical beams that do not alter with time. Recently, Rego et al.[91] demonstrated the extreme ultraviolet self-torqued beams in high-harmonic generation, as shown in Figs. 7(a)–7(c). Furthermore, the property of temporal OAM variation can be used to achieve ultrafast chiral excitations for light–matter interaction.[92] The self-torqued beams have time-varying longitudinal OAM based on the non-linear high-harmonic generation process. These examples exploited the ultrafast variations of longitudinal OAM.

The spatiotemporal vortex with transverse OAM provides a straightforward alternative to construct time-varying OAM beams linearly.[93] The dynamic-transverse-OAM beam embeds multiple spatiotemporal vortices of individually controllable topological charge in a wave packet. To create such a wave packet, a more complicated phase modulation hosting two phase singularities is applied rather than introducing a twisted phase in the spatiotemporal frequency plane. Figures 7(d) and 7(e) show the generation of an ultrafast wave packet embedded with two spatiotemporal vortices of topological charges 1 and −1, respectively. The spatiotemporal vortices carry an OAM of $\hbar$ and $-\hbar$ per photon. Moreover, Fig. 7(d) shows the interference patterns of the chirped wave packet slices with a short-probe pulse. The characteristics of bending fringes verify the topological charge of the two spatiotemporal vortices. The temporal separation of the two spatiotemporal vortices can be accurately manipulated from about 0.5 to 1 ps.[93] More complicated phase modulation in the spatiotemporal frequency plane and a broader bandwidth of the gain material will enable more spatiotemporal vortices to be embedded in one wave packet. Therefore, the dynamic-transverse-OAM beams may be utilized as ultrafast optical switches for high-speed optical communication.

## 7 Exemplary Applications of Engineered Photonic Angular Momentum

Photonic SAM and OAM states have spurred substantial theoretical and experimental research with broad applications in both classical and quantum optics, owing to their unique properties when interacting with matter. We will briefly introduce several representative applications of the angular momentum of light that have gained increasing attentions recently.

### 7.1 Optical Tweezers

Optical tweezers are effective tools in manipulating various micro- or nanoparticles by exerting optical forces on them through light–matter interactions.[94–98] SAM causes a microscopic object to spin around its own axis, while OAM causes the particle to revolve around the beam axis, owing to the rotational torque transferred from AM of the light to these objects.[19,99,100] Numerous studies have been conducted to enhance the performance of optical tweezers with the AM of light. The 3D optical tweezer can be constructed by employing an interferometric pattern between two annular optical fileds.[101] Through spin and orbital interactions, SAM carried by the circularly polarized beam can be used to make the trapped spherical microparticles orbit around the beam axis.[102,103] As shown in Fig. 8(a), the optical vortex with a high topological charge drives the particles to orbit around its ring by imposing scattering force on these particles.[104] The plasmonic vortex (PV) tweezer is exploited to stably trap the metal particles and overcome the strong absorption and scattering of metal particles, as shown in Fig. 8(b).[105] The azimuthal scattering force produced by the OAM of PV could manipulate the particles with higher precision in both radius and position. Moreover, optical torques induced by a surface plasmon can achieve the transverse spinning of the particle,[32] as shown in Fig. 8(c). In addition, optical tweezers based on a coaxial plasmonic aperture with circularly polarized illumination [as shown in Fig. 8(d)] could be utilized to selectively trap enantiomers, which can potentially realize all-optical enantiopure syntheses.[106]

### 7.2 Directional Coupling and Emission via Spin–Orbital Interactions

A significant application of transverse SAM is used to achieve spin-controlled directional propagation of light in a variety of situations.[107] Particularly, the near-field guided electromagnetic modes could be unidirectionally excited using the interference of a circularly polarized dipole for surface plasmon polariton waves, which determines the radiation direction in far fields, as shown in Fig. 9(a).[108] In addition, the incident photons with different polarization states can be spatially sorted into tridirectional routing by employing a specially designed triangular nanoparticle.[109] The integrated nanoscale spintronic components can be implemented based on spin-controlled optical modes through designing the symmetries of the metamaterial.[110] The spin of the optical field generated by a hyperbolic metasurface

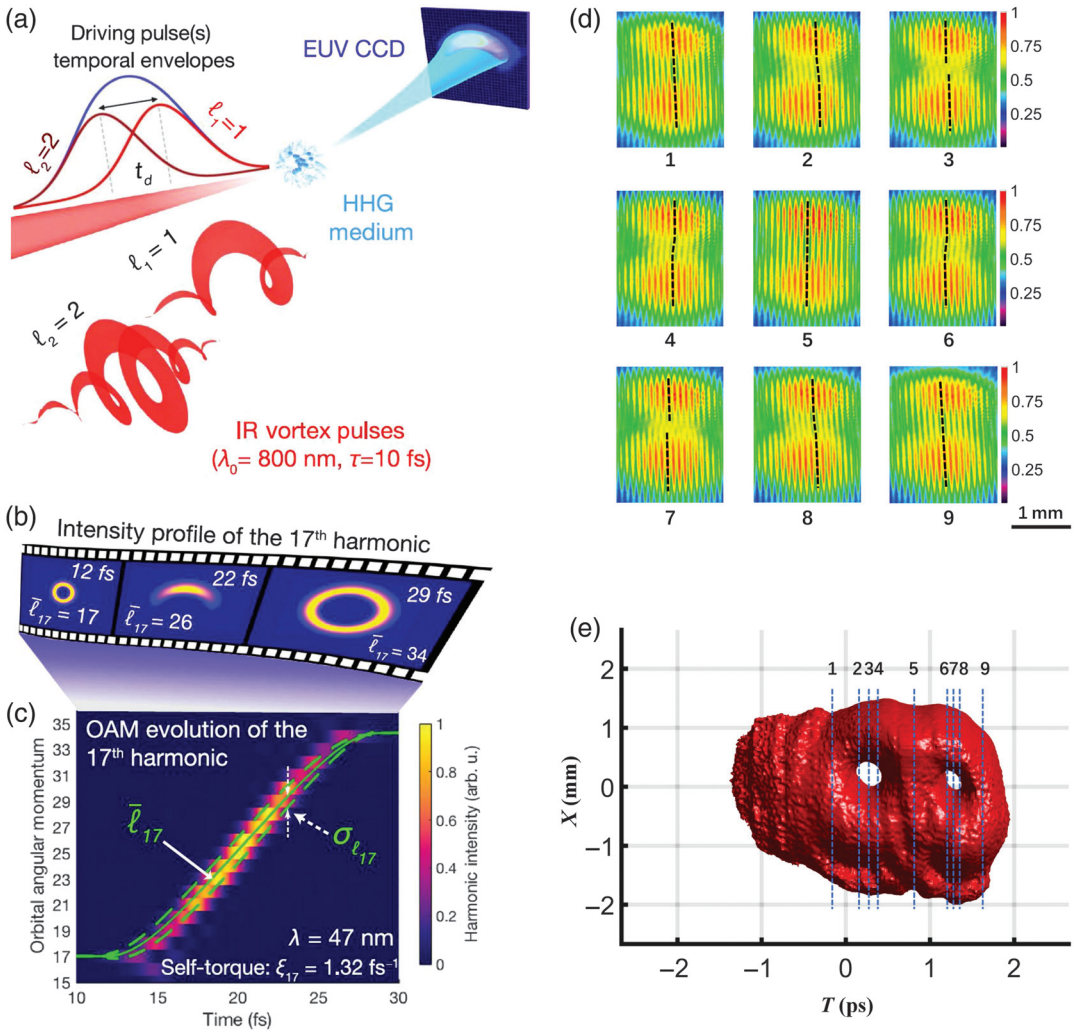


**Fig. 7** Ultrafast optical beams with time-varying OAM. (a) Two time-delayed, collinear pulses with different OAM values are focused into a gas target to produce self-torque beams. (b) Theoretical evolution of the intensity profile of the 17th harmonic at three temporal instants. (c) Evolution of the OAM of the 17th harmonic. (d) Interference fringe patterns of a chirped wave packet embedded with two spatiotemporal vortices with a short probe pulse. (e) 3D iso-intensity reconstruction of a wave packet containing two spatiotemporal vortices with temporal separation of 1 ps. Panels (a)–(c) are reproduced with permission from Ref. 91. Panels (d) and (e) are reproduced with permission from Ref. 93.

could be designed to orientate along an arbitrary direction, which could be applied to optically controlled SAM transfer.[111]

In the waveguide, the SAM of the excited beam specifies the coupled waveguide mode propagation direction. As shown in Figs. 9(b)–9(d), the propagation direction of the scattered light in the nanofiber is determined by both the nanoparticle azimuthal position on the surface of the fiber and the incident light polarization. In particular, the transverse SAM of the incident light with respect to the configuration enables directional radiation, where the radiation direction is determined by the chirality of the incident light.[112] Furthermore, directional coupling associated with transverse SAM has been exploited to fully control the optical polarization state in a single-mode nanofiber waveguide.[57] The tightly focused radially polarized field, which contains the transverse SAM that is crucial in manipulating the direction of the scattered field from the particle,[113] has been employed to excite a dipole-like nanoparticle to experimentally demonstrate the all-optical control of its directional emission. In addition, the spin–orbit interactions in suitable optical media can be employed to develop multi-channel non-reciprocal waveguide,[114] on-chip optimal Stokes nanopolarimetry,[115] and on-chip spin Hall devices.[116]

### 7.3 Optical Information Transmission and Processing

As shown in Fig. 10(a), photons have various physical degrees of freedom, including time, amplitude, polarization, spatial structure, and frequency/wavelength, which are widely adopted in optical communications as information carriers.[117,118] The multiplexing techniques of each dimension lead to wavelength-division multiplexing, time-division multiplexing, quadrature amplitude modulation, polarization-division multiplexing, mode-division multiplexing, etc.[119] The AM multiplexing modulation considerably enhances the capacity of optical communications

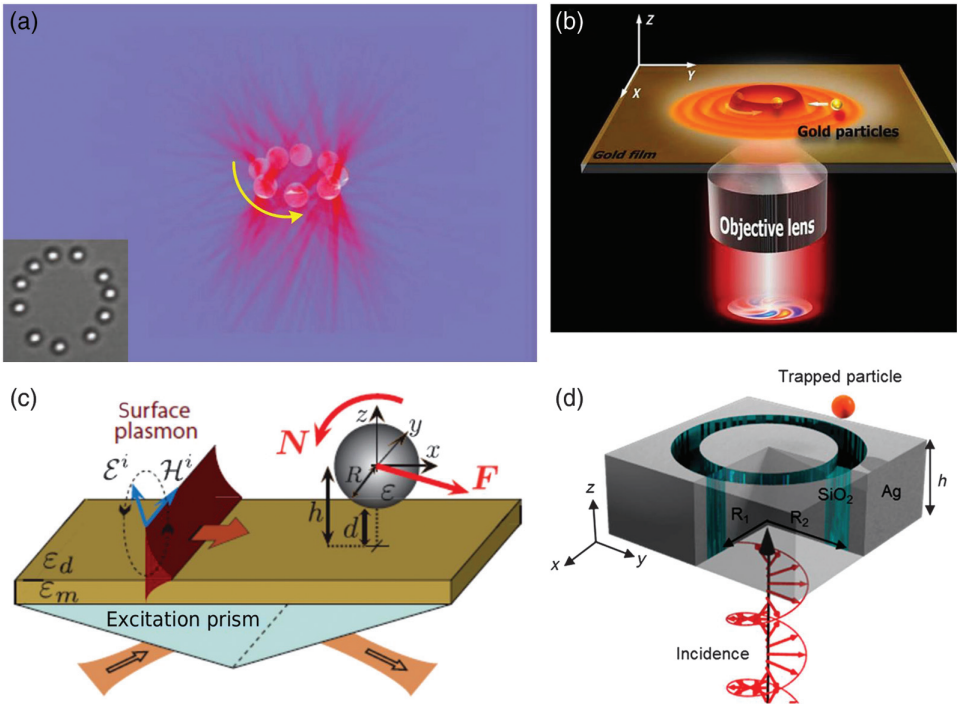


**Fig. 8** Optical manipulation employing photonic AM. (a) Microscopic beads orbit in the optical vortex. (b) Metal particles manipulated with the PV tweezers. (c) Transverse spinning of a particle caused by the surface plasmonic field. (d) Schematic of enantioselective optical trapping with plasmonic tweezers. Panel (a) is reproduced with permission from Ref. 104, (b) is reproduced with permission from Ref. 105, (c) is reproduced with permission from Ref. 32, and (d) is reproduced with permission from Ref. 106.

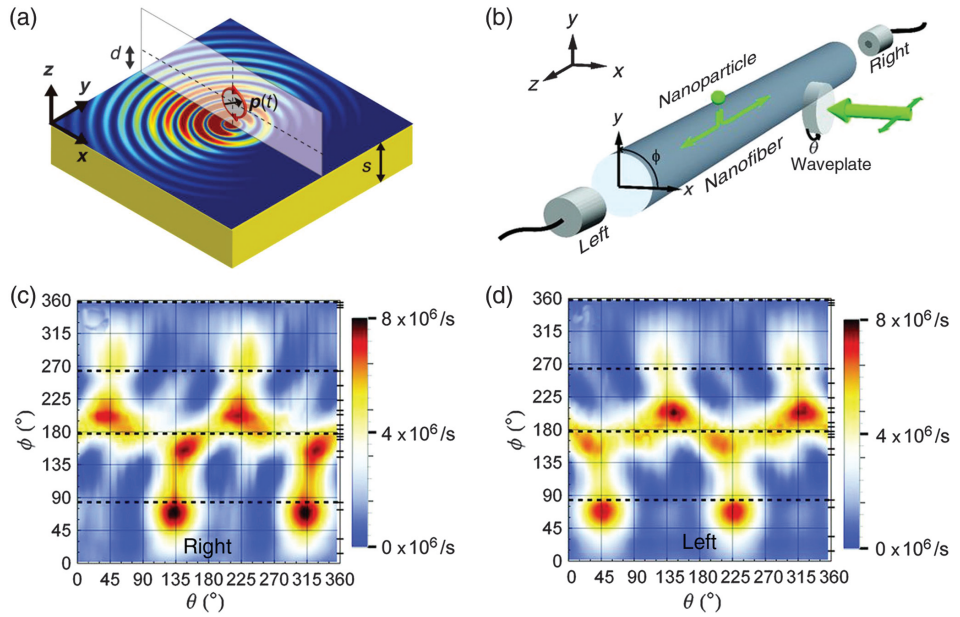


**Fig. 9** Spin-controlled directional coupling. (a) Asymmetric excitation of surface plasmon polariton wave. (b) Light with different polarizations coupled into a nanofiber via a nanoparticle. Experimental results of the scattered light at the right (c) and left (d) side of the nanofiber as a function of the nanoparticle position on the surface of the fiber and incident light polarization. Panel (a) is reproduced with permission from Ref. 108; (b)–(d) are reproduced with permission from Ref. 112.

because of the added degree of freedom given by the photonic AM.[120–122] It has been reported that the OAM multiplexing technique increases the capacity of free-space communication and optical fiber transmission systems higher than terabit scale,[123,124] much beyond the conventional scheme. More recently, the independent generation, transmission, and simultaneous detection of collinear OAM channels have been realized using Dammann optical vortex gratings, which offers a route to achieving Pbit $s^{-1}$ capacity for optical communication systems.[125] Moreover, various methods continue to emerge in OAM multiplexing communications. The retrieval array for optical vortices modulated in a sidelobe is employed to decode the data carried by a composite computer-generated hologram and to moderate the severe alignment and phase-matching required in detecting optical vortices.[126] On the other hand, OAM multiplexing can be adapted to increase the capacity of free space optical links between the ground station and unmanned aerial vehicle (UAV), as shown in Fig. 10(b), reducing the possibility of information interception.[127] Furthermore, the shape-invariant Bessel beams embedded with OAM provide higher power efficiency and longer reconstruction distances for free-space optical communication systems.[128] A scattering-matrix-assisted retrieval technique [SMART, as shown in Fig. 10(c)] was developed to demultiplex 24 OAM channels from greatly scattered light beams in a turbulent environment.[129] In fiber communications, it has been demonstrated that four modulated OAM mode groups can transmit over 2.6 km in traditional graded index multimode fibers.[130] An integrated OAM multiplexer/demultiplexer was demonstrated through fabrication of a vortex grating on the few-mode fiber facet, empowering the straight multiplexing and demultiplexing of OAM states between the two ports of the fiber.[131] Additionally, SAM and OAM of light can also be applied in quantum communication. For example, chiral SAM and OAM eigenstates are exploited to efficiently encode and decode the quantum information carried in rotationally invariant photonic qubits, to achieve alignment-free quantum communication.[132]

## 8 Conclusions and Future Perspectives

Photons carry angular momentum including spin and orbital components. In past decades, longitudinal SAM and OAM with momentum parallel to the Poynting vector are commonly studied, while the emerging transverse SAM has received numerous recent attentions in tightly focused beams and evanescent waves. Moreover, recent theoretical and experimental studies show the existence of transverse optical OAM in both free space and localized fields. In this review, we have summarized recent research progress in photonic AM, specifically, the advances in transverse SAM and OAM engineering. We presented methods to generate arbitrarily photonic SAM orientation in the tightly confined fields through purposefully and carefully engineering the spatial structure of incident pupil fields of high NA lens. The exotic 3D polarization topology (i.e., the optical polarization Möbius strip) was also reviewed to illustrate the capability of producing more sophisticated polarization or spin structures. Moreover, it is important to emphasize that the aforementioned examples were chosen to highlight that the structured light with an extraordinarily high-dimensional degree of freedom now enables scientists and researchers to produce photonic AM states traditionally unimaginable and to tailor photonic AM as desired to meet specific applications needs. As a fast-emerging field, it is certain that many significant works and applications other than those mentioned here have not been covered, including the applications of AM in non-linear optics, nanotechnology, optical machining, metrology, microscopy, and astronomy.[133]

Furthermore, recent breakthroughs in the spatiotemporal vortex with transverse OAM deserve special attention. In the quest for transverse OAM, it is important to note that the structuring of light in the temporal and spatiotemporal domains can be introduced in surprisingly simple ways. Adding temporal structure to the spatially complex optical field as the fifth degree of freedom (the other four degrees of freedom are phase, amplitude,

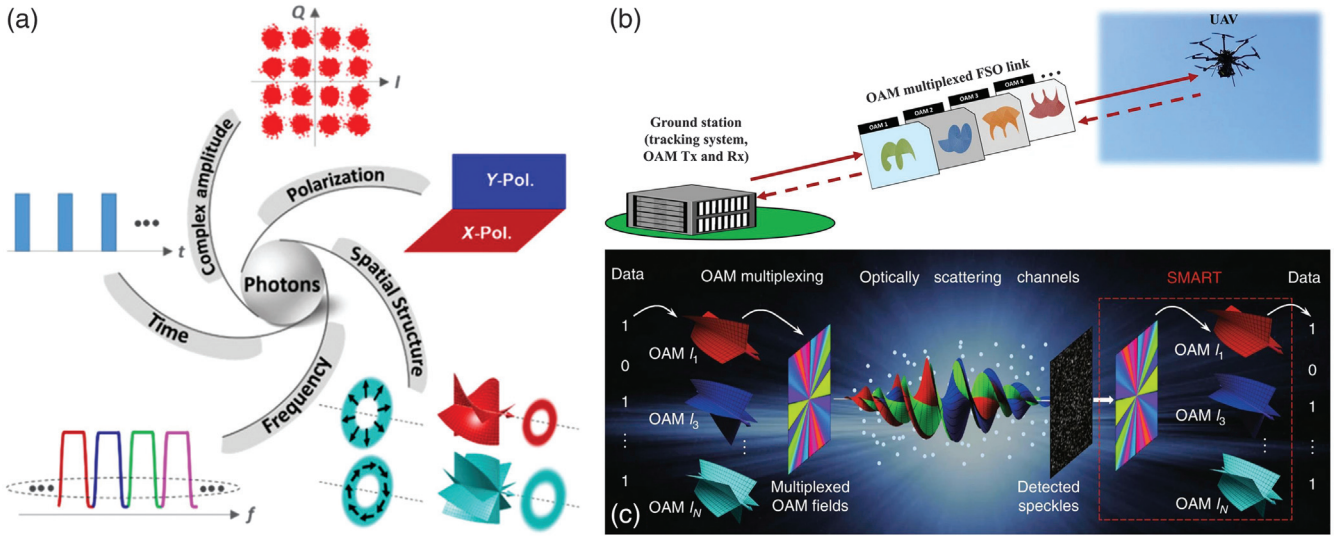


**Fig. 10** Optical communication using OAM of light. (a) Physical degrees of freedom of photons used in optical communication. (b) The schematic of optical communication between an UAV and a ground station utilizing OAM multiplexing. (c) OAM demultiplexing in a turbulent environment based on the SMART technique. Panel (a) is reproduced with permission from Ref. 117, (b) is reproduced with permission from Ref. 127, and (c) is reproduced with permission from Ref. 129.

polarization ratio, and ellipticity) in a controllable way represents a major leap forward. Investigations on transverse OAMs to understand their propagation, focusing, manipulation, and interaction with matter are still limited due to their complex nature. However, we believe more exciting developments are already on the horizon and anticipate a dramatic increase of research interest in this nascent area. A noteworthy research hotspot is in classical entanglement with structured light. Entanglement used to be discussed strictly in the quantum context. Recently, there has been much interest in constructing mathematically "non-separable" states using classical optical fields in the hope of retaining some of the features that are analogous to quantum entanglement, avoiding the drawbacks and pushing the quantum-classical boundary. The degrees of freedom of photonic AMs (polarization and OAM) embedded in structured light enable the generation and manipulation of higher-dimensional classical entanglements.[134] Furthermore, the inherent mathematical non-separability of spatiotemporally structured light makes it a natural candidate for the next forefront of entanglement studies.[135]

The rapid advances made in nanostructured materials offer synergy with the high-order degrees of freedom provided by the spatially and spatiotemporally structured light. As important characteristics of optical fields, photonic AMs play a significant role in light–matter interactions. Here, we list several directions that are emerging or have already made very recent breakthroughs.

(a) *Development of comprehensive non-linear toolboxes for photonic AM conversion and manipulation*. Structured light propagation through non-linear crystals, which has been employed to produce fast varying longitudinal OAM and self-torque light pulses,[91] has been studied in the context of OAM conservation. Moreover, there are also very recent reports on the second harmonic generation of transverse OAM.[136,137]

(b) *Coupling between tailored SAM and OAM*. Traditionally, spin–orbital coupling is studied between longitudinal SAM and OAM. However, coupling between longitudinal SAM and spatiotemporal OAM has been recently reported and revealed different dynamics,[88,89] which leads to the expectation of new coupling phenomena for tailored photonic AM and OAM states.

(c) *Coupled photonic AMs in materials interactions and super-resolution imaging*. The interactions of these newly coupled photonic AMs with nanostructures and materials may enable novel optical designs with functionalities that are difficult to implement traditionally. For example, photonic OAM has been investigated to significantly enhance the Raman activity of Raman spectroscopy.[138] Moreover, the coupling of photonic AMs has demonstrated promising applications in developing new super-resolution schemes.[139,140]

It is always very difficult, if not impossible, to predict the future for a rapidly developing field such as photonic AM. However, combined with the most recent progress in tailoring the spatial and temporal structure of optical fields, the studies of photonic AMs and their interactions with nanostructures and nanoemitters will certainly result in novel applications, including but not limited to advanced microscopy, laser machining, photonic chip, and quantum information processing.

## Acknowledgments

This work was supported by the National Natural Science Foundation of China (Nos. 92050202, 61805142, and 61875245), Shanghai Science and Technology Committee (No. 19060502500), and Shanghai Natural Science Foundation (No. 20ZR1437600). The authors declare no conflicts of interest.

## References

1. A. Forbes, M. de Oliveira, and M. R. Dennis, "Structured light," *Nat. Photonics* **15**(4), 253–262 (2021).
2. L. Allen, S. M. Barnett, and M. J. Padgett, *Optical Angular Momentum*, Institute of Physics Publishing, Bristol (2003).
3. D. L. Andrews and M. Babiker, *The Angular Momentum of Light*, Cambridge University Press, Cambridge (2013).
4. S. J. van Enk and G. Nienhuis, "Spin and orbital angular-momentum of photons," *Europhys. Lett.* **25**(7), 497–501 (1994).
5. S. Franke-Arnold, L. Allen, and M. Padgett, "Advances in optical angular momentum," *Laser Photonics Rev.* **2**(4), 299–313 (2008).
6. J. H. Poynting, "The wave motion of a revolving shaft, and a suggestion as to the angular momentum in a beam of circularly polarised light," *Proc. R. Soc. Lond. A* **82**, 560–567 (1909).
7. R. A. Beth, "Mechanical detection and measurement of the angular momentum of light," *Phys. Rev.* **50**(2), 115–125 (1936).
8. K. Y. Bliokh et al., "Spin–orbit interactions of light," *Nat. Photonics* **9**(12), 796–808 (2015).
9. L. Allen et al., "Orbital angular-momentum of light and the transformation of Laguerre–Gaussian laser modes," *Phys. Rev. A* **45**(11), 8185–8189 (1992).
10. H. He et al., "Direct observation of transfer of angular-momentum to absorptive particles from a laser beam with a phase singularity," *Phys. Rev. Lett.* **75**(5), 826–829 (1995).
11. A. Bekshaev, K. Y. Bliokh, and M. Soskin, "Internal flows and energy circulation in light beams," *J. Opt.* **13**(5), 053001 (2011).
12. V. Y. Bazhenov, M. V. Vasnetsov, and M. S. Soskin, "Laser beams with screw dislocations in their wavefronts," *JETP Lett.* **52**(8), 429–431 (1990).
13. A. S. Desyatnikov, Y. S. Kivshar, and L. Torner, "Optical vortices and vortex solitons," *Prog. Opt.* **47**, 291–391 (2005).
14. M. R. Dennis, K. O'Holleran, and M. J. Padgett, "Singular optics: optical vortices and polarization singularities," *Prog. Opt.* **53**, 293–363 (2009).
15. K. Y. Bliokh, A. Aiello, and M. A. Alonso, *Spin-Orbit Interactions of Light in Isotropic Media*, pp. 174–245, Cambridge University Press, Cambridge (2012).
16. L. Allen, M. J. Padgett, and M. Babiker, "The orbital angular momentum of light," *Prog. Opt.* **39**, 291–372 (1999).
17. G. Molina-Terriza, J. P. Torres, and L. Torner, "Twisted photons," *Nat. Phys.* **3**(5), 305–310 (2007).
18. A. M. Yao and M. J. Padgett, "Optical angular momentum: origins, behavior, and applications," *Adv. Opt. Photonics* **3**(2), 161–204 (2011).
19. A. T. O'Neil et al., "Intrinsic and extrinsic nature of the orbital angular momentum of a light beam," *Phys. Rev. Lett.* **88**(5), 053601 (2002).
20. Y. Zhao et al., "Spin-to-orbital angular momentum conversion in a strongly focused optical beam," *Phys. Rev. Lett.* **99**(7), 073901 (2007).
21. E. Wigner, "On unitary representations of the inhomogeneous Lorentz group," *Ann. Math.* **40**(1), 149–204 (1939).
22. T. D. Newton and E. P. Wigner, "Localized states for elementary systems," *Rev. Mod. Phys.* **21**(3), 400–406 (1949).
23. L. Mandel and E. Wolf, *Optical Coherence and Quantum Optics*, Cambridge University Press, Cambridge (1995).
24. J. F. Nye and M. V. Berry, "Dislocations in wave trains," *Proc. R. Soc. Lond. Ser. A* **336**, 165–190 (1974).

25. D. Sarenac et al., "Direct discrimination of structured light by humans," *P. Natl. Acad. Sci. U. S. A.* **117**(26), 14682–14687 (2020).
26. M. S. Soskin and M. V. Vasnetsov, "Singular optics," *Prog. Opt.* **42**, 219–276 (2001).
27. W. Zhu et al., "Transverse spin angular momentum of tightly focused full Poincaré beams," *Opt. Express* **23**(26), 34029–34041 (2015).
28. K. Y. Bliokh, D. Smirnova, and F. Nori, "Quantum spin Hall effect of light," *Science* **348**(6242), 1448–1451 (2015).
29. M. H. Alizadeh and B. M. Reinhard, "Emergence of transverse spin in optical modes of semiconductor nanowires," *Opt. Express* **24**(8), 8471–8479 (2016).
30. P. Woźniak et al., "Tighter spots of light with superposed orbital-angular-momentum beams," *Phys. Rev. A* **94**(2), 021803 (2016).
31. J. Chen, C. Wan, and Q. Zhan, "Vectorial optical fields: recent advances and future prospects," *Sci. Bull.* **63**(1), 54–74 (2018).
32. A. Canaguier-Durand and C. Genet, "Transverse spinning of a sphere in a plasmonic field," *Phys. Rev. A* **89**(3), 033841 (2014).
33. M. Neugebauer et al., "Magnetic and electric transverse spin density of spatially confined light," *Phys. Rev. X* **8**(2), 021042 (2018).
34. M. Sotto et al., "Spin-orbit coupling of light in photonic crystal waveguides," *Phys. Rev. A* **99**(5), 053845 (2019).
35. J. Chen, D. Zhang, and Q. Zhan, "Effective iterative method for accurate amplitude modulation in complex optical field generation," *Opt. Eng.* **58**(8), 082404 (2019).
36. W. Miao, X. Pang, and W. Liu, "Photonic wheels and their topological reaction in a strongly focused amplitude tailored beam," *IEEE Photonics J.* **12**(2), 6500709 (2020).
37. S. He et al., "Spatial differential operation and edge detection based on the geometric spin Hall effect of light," *Opt. Lett.* **45**(4), 877–880 (2020).
38. M. Mahankali et al., "Spectral singularity enhances transverse spin," *Opt. Commun.* **454**, 124433 (2020).
39. D. R. Abujetas and J. A. Sánchez-Gil, "Spin angular momentum of guided light induced by transverse confinement and intrinsic helicity," *ACS Photonics* **7**(2), 534–545 (2020).
40. Z. Man, X. Dou, and H. P. Urbach, "The evolutions of spin density and energy flux of strongly focused standard full Poincaré beams," *Opt. Commun.* **458**, 124790 (2020).
41. N. Jhajj et al., "Spatiotemporal optical vortices," *Phys. Rev. X* **6**(3), 031037 (2016).
42. A. Aiello et al., "From transverse angular momentum to photonic wheels," *Nat. Photonics* **9**(12), 789–795 (2015).
43. E. Wolf, "Electromagnetic diffraction in optical systems I. An integral representation of the image field," *Proc. R. Soc. A* **253**(1274), 349–357 (1959).
44. B. Richards and E. Wolf, "Electromagnetic diffraction in optical system II. Structure of the image field in an aplanatic system," *Proc. R. Soc. A* **253**(1274), 358–379 (1959).
45. K. Y. Bliokh, A. Y. Bekshaev, and F. Nori, "Extraordinary momentum and spin in evanescent waves," *Nat. Commun.* **5**(1), 3300 (2014).
46. P. Banzer et al., "The photonic wheel: demonstration of a state of light with purely transverse angular momentum," *J. Eur. Opt. Soc. Rap. Public.* **8**, 13032 (2013).
47. J. Chen et al., "Experimental generation of complex optical fields for diffraction limited optical focus with purely transverse spin angular momentum," *Opt. Express* **25**(8), 8966–8974 (2017).
48. A. Y. Bekshaev, K. Y. Bliokh, and F. Nori, "Transverse spin and momentum in two-wave interference," *Phys. Rev. X* **5**(1), 011039 (2015).
49. S. Saha et al., "Transverse spin and transverse momentum in scattering of plane waves," *Opt. Lett.* **41**(19), 4499–4502 (2016).
50. K. Y. Bliokh and F. Nori, "Transverse spin of a surface polariton," *Phys. Rev. A* **85**(6), 061801 (2012).
51. K. Y. Kim et al., "Time reversal and the spin angular momentum of transverse-electric and trans-verse-magnetic surface modes," *Phys. Rev. A* **86**(6), 063805 (2012).
52. D. O'Connor et al., "Spin–orbit coupling in surface plasmon scattering by nanostructures," *Nat. Commun.* **5**(1), 5327 (2014).
53. L. Marrucci, "Spin gives direction," *Nat. Phys.* **11**, 9–10 (2015).
54. A. B. Young et al., "Polarization engineering in photonic crystal waveguides for spin-photon entanglers," *Phys. Rev. Lett.* **115**(15), 153901 (2015).
55. I. Söllner et al., "Deterministic photon-emitter coupling in chiral photonic circuits," *Nat. Nanotechnol.* **10**(9), 775–778 (2015).
56. M. F. Picardi et al., "Angular momenta, helicity, and other properties of dielectric-fiber and metallic-wire modes," *Optica* **5**(8), 1016–1026 (2018).
57. F. Lei et al., "Complete polarization control for a nanofiber waveguide using directional coupling," *Phys. Rev. Appl.* **11**(6), 064041 (2019).
58. R. Mitsch et al., "Quantum state-controlled directional spontaneous emission of photons into a nanophotonic waveguide," *Nat. Commun.* **5**, 5713 (2014).
59. L. Hang, P. Chen, and Y. Wang, "Theoretical generation of arbitrarily homogeneously 3D spin-orientated optical needles and chains," *Opt. Express* **27**(5), 6047–6056 (2019).
60. K. Y. Bliokh and F. Nori, "Spatiotemporal vortex beams and angular momentum," *Phys. Rev. A* **86**(3), 033824 (2012).
61. A. Chong et al., "Generation of spatiotemporal optical vortices with controllable transverse orbital angular momentum," *Nat. Photonics* **14**(6), 350–354 (2020).
62. S. W. Hancock et al., "Free-space propagation of spatiotemporal optical vortices," *Optica* **6**(12), 1547–1553 (2019).
63. J. Chen et al., "Subwavelength focusing of spatio-temporal wave packet with transverse orbital angular momentum," *Opt. Express* **28**(12), 18472–18478 (2020).
64. K. Y. Bliokh, A. Y. Bekshaev, and F. Nori, "Optical momentum, spin, and angular momentum in dispersive media," *Phys. Rev. Lett.* **119**(7), 073901 (2017).
65. Y. Shen et al., "Optical vortices 30 years on: OAM manipulation from topological charge to multiple singularities," *Light Sci. Appl.* **8**(1), 90 (2019).
66. K. Y. Bliokh and F. Nori, "Transverse and longitudinal angular momenta of light," *Phys. Rep.* **592**, 1–38 (2015).
67. K. Y. Bliokh, J. Dressel, and F. Nori, "Conservation of the spin and orbital angular momenta in electromagnetism," *New J. Phys.* **16**(9), 093037 (2014).
68. R. P. Cameron and S. M. Barnett, "Electric-magnetic symmetry and Noether's theorem," *New J. Phys.* **14**(12), 123019 (2012).
69. M. V. Berry, "Optical currents," *J. Opt. A: Pure Appl. Opt.* **11**(9), 094001 (2009).
70. R. P. Cameron, S. M. Barnett, and A. M. Yao, "Optical helicity, optical spin, and related quantities in electromagnetic theory," *New J. Phys.* **14**(5), 053050 (2012).
71. R. M. A. Azzam and N. M. Bashara, *Ellipsometry and Polarized Light*, North-Holland Publishing Company, Amsterdam (1977).
72. M. Neugebauer et al., "Geometric spin Hall effect of light in tightly focused polarization-tailored light beams," *Phys. Rev. A* **89**(1), 013840 (2014).
73. W. Chen and Q. Zhan, "Diffraction limited focusing with controllable arbitrary three-dimensional polarization," *J. Opt.* **12**(4), 045707 (2010).
74. Q. Zhan, "Cylindrical vector beams: from mathematical concepts to applications," *Adv. Opt. Photonics* **1**(1), 1–57 (2009).
75. J. Chen et al., "Tightly focused optical field with controllable photonic spin orientation," *Opt. Express* **25**(16), 19517–19528 (2017).
76. C. A. Balanis, *Antenna Theory: Analysis and Design*, John Wiley & Sons Inc., Hoboken (2005).

77. M. Berry, "Index formulae for singular lines of polarization," *J. Opt. A: Pure Appl. Opt.* **6**(7), 675–678 (2004).
78. T. Bauer et al., "Optical polarization Möbius strips and points of purely transverse spin density," *Phys. Rev. Lett.* **117**(1), 013601 (2016).
79. T. Bauer et al., "Observation of optical polarization Möbius strips," *Science* **347**(6225), 964–966 (2015).
80. L. Marrucci, C. Manzo, and D. Paparo, "Optical spin-to-orbital angular momentum conversion in inhomogeneous anisotropic media," *Phys. Rev. Lett.* **96**(16), 163905 (2006).
81. A. Garcia-Etxarri, "Optical polarization Möbius strips on all-dielectric optical scatterers," *ACS Photonics* **4**(5), 1159–1164 (2017).
82. C. Wan and Q. Zhan, "Generation of exotic optical polarization Möbius strips," *Opt. Express* **27**(8), 11516–11524 (2019).
83. M. Leutenegger et al., "Fast focus field calculations," *Opt. Express* **14**(23), 11277–11291 (2006).
84. J. V. Cornacchio and R. P. Soni, "On a relation between two-dimensional Fourier integrals and series of Hankel transforms," *J. Res. Natl. Bureau Standards B* **69B**(3), 173–174 (1965).
85. A. M. Weiner, "Femtosecond pulse shaping using spatial light modulators," *Rev. Sci. Instrum.* **71**(5), 1929–1960 (2000).
86. H. Li et al., "Three-dimensional laser pulse intensity diagnostic for photoinjectors," *Phys. Rev. ST Accel. Beams* **14**(11), 112802 (2011).
87. C. Wan et al., "Experimental demonstration of ultrafast wave-packet containing orbital angular momentum with controllable orientation," *Natl. Sci. Rev.*, nwab149 (2021).
88. J. Chen et al., "Spin-orbit coupling within tightly focused circularly polarized spatiotemporal vortex wavepacket," https://arxiv.org/abs/2103.09467 (2021).
89. K. Y. Bliokh, "Spatiotemporal vortex pulses: angular momenta and spin-orbit interaction," *Phys. Rev. Lett.* **126**(24), 243601 (2021).
90. J. Chen et al., "Experimental generation of cylindrical vector spatiotemporal optical vortex," https://arxiv.org/abs/2101.09452 (2021).
91. L. Rego et al., "Generation of extreme-ultraviolet beams with time-varying orbital angular momentum," *Science* **364**(6447), eaaw9486 (2019).
92. R. M. Kerber et al., "Orbital angular momentum dichroism in nanoantennas," *Commun. Phys.* **1**(1), 87 (2018).
93. C. Wan et al., "Generation of ultrafast spatiotemporal wave packet embedded with time-varying orbital angular momentum," *Sci. Bull.* **65**(16), 1334–1336 (2020).
94. P. C. Chaumet and M. Nieto-Vesperinas, "Time-averaged total force on a dipolar sphere in an electromagnetic field," *Opt. Lett.* **25**(15), 1065–1067 (2000).
95. D. G. Grier, "A revolution in optical manipulation," *Nature* **424**(6950), 810–816 (2003).
96. F. Nan and Z. Yan, "Synergy of intensity, phase, and polarization enables versatile optical nanomanipulation," *Nano Lett.* **20**(4), 2778–2783 (2020).
97. Y. Yuan et al., "Advances on studying optical forces: optical manipulation, optical cooling and light induced dynamics," *J. Phys. D Appl. Phys.* **53**(28), 283001 (2020).
98. K. Lin et al., "Spatiotemporal rotational dynamics of laser-driven molecules," *Adv. Photonics* **2**(2), 024002 (2020).
99. L. Paterson et al., "Controlled rotation of optically trapped microscopic particles," *Science* **292**(5518), 912–914 (2001).
100. V. Garcés-Chávez et al., "Observation of the transfer of the local angular momentum density of a multiringed light beam to an optically trapped particle," *Phys. Rev. Lett.* **91**(9), 093602 (2003).
101. M. P. MacDonald et al., "Creation and manipulation of three-dimensional optically trapped structures," *Science* **296**(5570), 1101–1103 (2002).
102. H. Adachi, S. Akahoshi, and K. Miyakawa, "Orbital motion of spherical microparticles trapped in diffraction patterns of circularly polarized light," *Phys. Rev. A* **75**(6), 063409 (2007).
103. G. Tkachenko, M. Rafayelyan, and E. Brasselet, "Spin-orbit optomechanics of optically levitated chiral Bragg microspheres," *Phys. Rev. A* **95**(5), 053839 (2017).
104. M. Padgett and R. Bowman, "Tweezers with a twist," *Nat. Photonics* **5**(6), 343–348 (2011).
105. Y. Zhang et al., "A plasmonic spanner for metal particle manipulation," *Sci. Rep.* **5**(1), 15446 (2015).
106. Y. Zhao, A. Saleh, and J. A. Dionne, "Enantioselective optical trapping of chiral nanoparticles with plasmonic tweezers," *ACS Photonics* **3**(3), 304–309 (2016).
107. F. Cardano and L. Marrucci, "Spin–orbit photonics," *Nat. Photonics* **9**(12), 776–778 (2015).
108. F. J. Rodríguez-Fortuño et al., "Near-field interference for the unidirectional excitation of electromagnetic guided modes," *Science* **340**(6130), 328–330 (2013).
109. Y. Tanaka and T. Shimura, "Tridirectional polarization routing of light by a single triangular plasmonic nanoparticle," *Nano Lett.* **17**(5), 3165–3170 (2017).
110. N. Shitrit et al., "Spin-optical metamaterial route to spin-controlled photonics," *Science* **340**(6133), 724–726 (2013).
111. Y. Yermakov et al., "Spin control of light with hyperbolic metasurfaces," *Phys. Rev. B* **94**(7), 075446 (2016).
112. J. Petersen, J. Volz, and A. Rauschenbeutel, "Chiral nanophotonic waveguide interface based on spin-orbit interaction of light," *Science* **346**(6205), 67–71 (2014).
113. M. Neugebauer et al., "Polarization tailored light driven directional optical nanobeacon," *Nano Lett.* **14**(5), 2546–2551 (2014).
114. H. Hu et al., "Routing emission with a multi-channel nonreciprocal waveguide," *Photonics Res.* **7**(6), 642–646 (2019).
115. A. Espinosa-Soria et al., "On-chip optimal Stokes nanopolarimetry based on spin–orbit interaction of light," *Nano Lett.* **17**(5), 3139–3144 (2017).
116. Z. Xie et al., "Broadband on-chip photonic spin Hall element via inverse design," *Photonics Res.* **8**(2), 121–126 (2020).
117. J. Wang, "Advances in communications using optical vortices," *Photonics Res.* **4**(5), B14–B28 (2016).
118. I. Gianani et al., "Transmission of vector vortex beams in dispersive media," *Adv. Photonics* **2**(3), 036003 (2020).
119. D. J. Richardson, J. M. Fini, and L. E. Nelson, "Space-division multiplexing in optical fibres," *Nat. Photonics* **7**(5), 354–362 (2013).
120. J. T. Barreiro, T. Wei, and P. G. Kwiat, "Beating the channel capacity limit for linear photonic superdense coding," *Nat. Phys.* **4**(4), 282–286 (2008).
121. A. Trichili et al., "Communicating using spatial mode multiplexing: potentials, challenges, and perspectives," *IEEE Commun. Surv. Tutorials* **21**(4), 3175–3203 (2019).
122. A. E. Willner et al., "Optical communications using orbital angular momentum beams," *Adv. Opt. Photonics* **7**(1), 66–106 (2015).
123. J. Wang et al., "Terabit free-space data transmission employing orbital angular momentum multiplexing," *Nat. Photonics* **6**(7), 488–496 (2012).
124. N. Bozinovic et al., "Terabit-scale orbital angular momentum mode division multiplexing in fibers," *Science* **340**(6140), 1545–1548 (2013).
125. T. Lei et al., "Massive individual orbital angular momentum channels for multiplexing enabled by Dammann gratings," *Light Sci. Appl.* **4**(3), e257 (2015).
126. P. Jia et al., "Sidelobe-modulated optical vortices for free-space communication," *Opt. Lett.* **38**(4), 588–590 (2013).
127. L. Li et al., "High-capacity free-space optical communications between a ground transmitter and a ground receiver via a UAV using multiplexing of multiple orbital-angular-momentum beams," *Sci. Rep.* **7**, 17427 (2017).
128. N. Mphuthi et al., "Free-space optical communication link with shape-invariant orbital angular momentum Bessel beams," *Appl. Opt.* **58**(16), 4258–4264 (2019).

129. L. Gong et al., "Optical orbital-angular-momentum-multiplexed data transmission under high scattering," *Light Sci. Appl.* **8**(1), 27 (2019).
130. L. Zhu et al., "Orbital angular momentum mode groups multiplexing transmission over 2.6-km conventional multi-mode fiber," *Opt. Express* **25**(21), 25637–25645 (2017).
131. Z. Xie et al., "Integrated (de)multiplexer for orbital angular momentum fiber communication," *Photonics Res.* **6**(7), 743–749 (2018).
132. V. D'Ambrosio, E. Nagali, and S. Walborn, "Complete experimental toolbox for alignment-free quantum communication," *Nat. Commun.* **3**, 961 (2012).
133. M. P. J. Lavery et al., "Detection of a spinning object using light's orbital angular momentum," *Science* **341**(6145), 537–540 (2013).
134. Y. Shen et al., "Creation and control of high-dimensional multipartite classically entangled light," *Light Sci. Appl.* **10**(1), 50 (2021).
135. Y. Shen et al., "Measures of space-time nonseparability of electromagnetic pulses," *Phys. Rev. Research* **3**(1), 013236 (2021).
136. G. Gui et al., "Second-harmonic generation and the conservation of spatiotemporal orbital angular momentum of light," *Nat. Photonics* **15**(8), 608–613 (2021).
137. S. W. Hancock, S. Zahedpour, and H. M. Milchberg, "Second harmonic generation of spatiotemporal optical vortices and conservation of orbital angular momentum," *Optica* **8**(5), 594–597 (2021).
138. K. A. Forbes, "Raman optical activity using twisted photons," *Phys. Rev. Lett.* **122**(10), 103201 (2019).
139. H. Hu, Q. Gan, and Q. Zhan, "Generation of a nondiffracting superchiral optical needle for circular dichroism imaging of sparse subdiffraction objects," *Phys. Rev. Lett.* **122**(22), 223901 (2019).
140. L. Du et al., "Deep-subwavelength features of photonic skyrmions in a confined electromagnetic field with orbital angular momentum," *Nat. Phys.* **15**(7), 650–654 (2019).

**Jian Chen** is an associate professor with special appointment at the University of Shanghai for Science and Technology. He received his PhD in signal and information processing from University of Electronic Science and Technology of China in 2017. His current research interests include complex optical field manipulation, and the interaction between the engineered optical fields and the nanostructures.

**Chenhao Wan** obtained his PhD in electrical engineering from the University of Minnesota. He is currently an associate professor at the School of Optical and Electronic Information of Huazhong University of Science and Technology. His research interests include structured light, laser beam combining, and diffractive optics.

**Qiwen Zhan** is a distinguished chair professor in nanophotonics at the University of Shanghai for Science and Technology and director for the Center for Complex Optical Fields and Meta-Optics Structures (COSMOS). He received his PhD in electrical engineering from the University of Minnesota in 2002. The current research in his group mainly focuses on complex optical fields and exploring their applications in nanophotonics, metrology, and biophotonics. He is an associate editor for *Optica* and an associate editor-in-chief for *PhotoniX*. He is an elected fellow of OSA, a fellow of SPIE, and a senior member of IEEE.